Strojnícky časopis – *Journal of* MECHANICAL ENGINEERING,
VOL 73 (2023), NO 1, 159 - 168

REAL TIME SWINGING UP AND STABILIZING A DOUBLE INVERTED PENDULUM USING PID-LQR

SHALA Erjon[1], BAJRAMI Xhevahir[1], LIKAJ Rame[1*], PAJAZITI Arbnor[1]

[1] Department of Mechatronics, Faculty of Mechanical Engineering, University of Pristina " Hasan Prishtina", 10000 Prishtina, Kosovo,
[*]Correspondence: rame.likaj@uni-pr.edu

Abstract: This study describes a method for swinging up and stabilizing a double inverted pendulum (DIP) in real-time utilizing a PID-LQR combined control system. Firstly, a dynamic model of the double inverted pendulum system is made up and the equations of motion are constructed. The pendulum then is moved from its unstable position to a stable one using a PID-LQR controller. A comparison of the PID-LQR controller's output and suggestions for improving system stability is presented and is suggested combined control system.

KEYWORDS: Real-time control, Double Inverted Pendulum, PID-LQR Control, Swing Up and Stabilization.

1 Introduction

The control system for swinging up and stabilizing a double inverted pendulum in real-time is introduced in this study. Due to its complex dynamics, the double inverted pendulum is a type of nonlinear system with numerous degrees of freedom. To move the pendulum from an unstable position to a stable one and increase the system's stability, a PID-LQR controller combination is suggested [1], [11]. The equations of motion of the double inverted pendulum system are derived and a dynamic model of the system is established [2]. The PID-LQR controller is designed to generate the control signal to swing up the pendulum [3]. Then, a neural network is used to learn the output of the PID-LQR controller and further improve the stability of the system. Simulation results demonstrate the effectiveness of the combined control system in swinging up and stabilizing the double inverted pendulum in real-time [4].

The double inverted pendulum is an example of a complex, nonlinear dynamic system. It consists of two inverted pendulums attached to each other at their respective centres of mass. This system is unstable and difficult to control, due to the presence of two degrees of freedom and the inherent nonlinearity. In this project, we aim to design a real-time control system that is capable of swinging up and stabilizing the double inverted pendulum using a combination of PID and LQR [5]. The PID-LQR controller is a classical approach to control, which is used to generate control signals that will swing up the pendulum and bring it to a stable equilibrium point. The system is then tested in real-time by simulating the double inverted pendulum in a simulation environment [6]. The results of the real-time simulation show that both the PID-LQR and neural network controllers were successful in swinging up and stabilizing the double inverted pendulum [7]. Overall, this project demonstrates the effectiveness of combining classical and modern control techniques to design a real-time control system for a complex, nonlinear dynamic system [12].

DOI: 10.2478/scjme-2023-0013, Print ISSN 0039-2472, On-line ISSN 2450-5471

2 Mathematical equations of the double inverted pendulum

The double pendulum model shown in Figure 1 has the DBPEN-LIN attached to the IP02 Linear Servo Base Unit [7]. The positive direction of rotation, when facing the linear cart pinions, is counter-clockwise (CCW) [7]. The zero angle of the pendulums, $\theta = 0$ and $\alpha = 0$, is defined to be when the two pendulums are perfectly balanced vertically and the positive direction of linear displacement of the IP02 cart is to the right when facing the cart [7].

Tab. 1 Notation and units of constant parameters of the DIP system [7]

Parameter	*Unit*	*Description*
m_c	[Kg]	Mass of the cart
m_{p1}, m_{p2}	[Kg]	Mass of the pendulums
l_1, l_2	[m]	Length of the pendulums
l_{p1}, l_{p2}	[m]	Distance from pivot joints to the pendulums' centre of mass
I_1, I_2	[Kg m^2]	Pendulums' moment of Inertia
g	m/s^2	Gravity constant
x_c	[m]	Cart position
α, θ	[rad]	Pendulums' angles

Figure 1 shows the schematic of DIP system on a cart which will be studied in this project

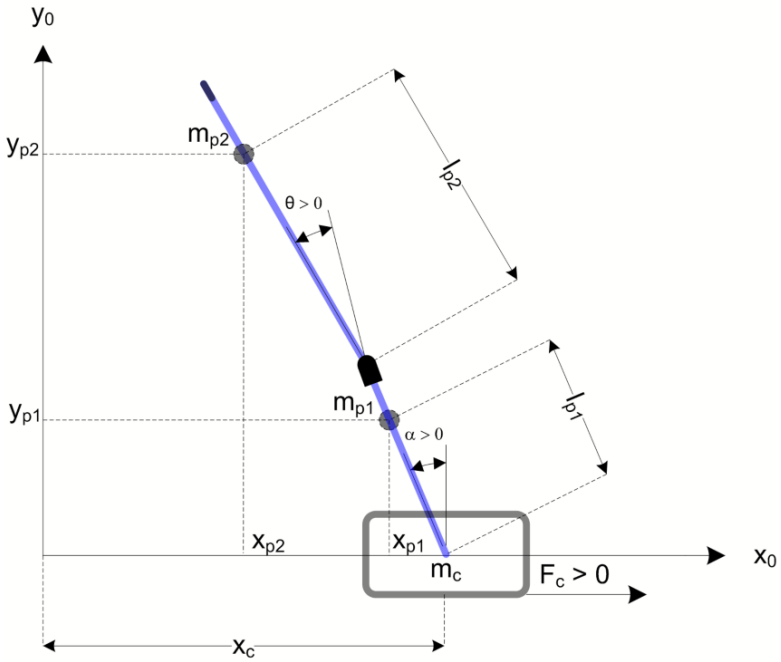


Fig. 1 Mathematical model of the DIP [7].

In this study the desired equations of motion are found by implementing Lagrange's equations:

$$\frac{d}{dt}\left(\frac{\partial T}{\partial \dot{q}}\right) - \frac{\partial T}{\partial q_i} = Q_i, where: i = [1, 2, 3 \cdots r] \tag{1}$$

where the q_i $i = [1, 2, 3 \cdots r]$ is a set of generalized coordinates, the generalized forces or moments acting in direction of coordinates Q_i can be denoted by forces, and the Lagrangian function T is defined as the product of the kinetic and potential energies:

$$T = E_k(q_1, q_2, \dots, q_r, \dot{q_1}, \dots, \dot{q_r}) - E_p(q_1, \dots, q_r) \tag{2}$$

in which E_k is the kinetic energy and E_p presents the potential energy. For the DIP system presented in Figure 1, the kinetic and potential energies can be determined by summing up the individual components' energies [7]. The independent coordinate parameters of the system are x_c, α and θ. Considering the external force F_c applied to the system along the x coordinate and ignoring the friction of the system, equation (1) can be expanded as follows:

$$\frac{d}{dt}\left(\frac{\partial T}{\partial \dot{x}_c}\right) - \frac{\partial T}{\partial x_c} = \mathrm{u} \tag{3}$$

$$\frac{d}{dt}\left(\frac{\partial T}{\partial \dot{\alpha}}\right) - \frac{\partial T}{\partial \alpha} = 0 \tag{4}$$

$$\frac{d}{dt}\left(\frac{\partial T}{\partial \dot{\theta}}\right) - \frac{\partial T}{\partial \theta} = 0 \tag{5}$$

The equation of motion for a double inverted pendulum (DIP) system can be written as:

$$T = \sum_{i=1}^{n} E_{k(1\cdots3)} - \sum_{j=1}^{m} E_{p(1\cdots3)} \tag{6}$$

$$\left.\begin{aligned} E_{k_{total}} &= E_k^{cart} + E_k^{pend_1} + E_k^{pend_2} \\ E_{p_{total}} &= E_p^{cart} + E_p^{pend_1} + E_p^{pend_2} \end{aligned}\right\} \tag{7}$$

$$\left.\begin{aligned} E_k^{cart} &= \frac{1}{2} m_c \dot{x}_c^2 \\ E_k^{pend_1} &= \frac{1}{2} m_1 \dot{x}_c^2 + \frac{1}{2}\left(m_{p1} l_{p1}^2 + I_{p1}\right)\dot{\alpha}^2 + m_{p1} l_{p1} \dot{x}_c \dot{\alpha}^2 \cos(\alpha) \\ E_k^{pend_2} &= \frac{1}{2} m_2 \dot{x}_c^2 + \frac{1}{2} m_{p2} l_1^2 \dot{\alpha}^2 + \frac{1}{2}\left(m_2 l_{p2}^2 + I_{p2}\right)\dot{\alpha}_2^2 + \\ & m_2 \dot{x}_c\left(l_1 \dot{\alpha} \cos(\alpha) + l_{p2} \dot{\theta} \cos(\theta)\right) + m_2 l_1 l_{p2} \dot{\alpha} \cdot \dot{\theta} \cos(\alpha - \theta) \end{aligned}\right\} \tag{8}$$

$$\left.\begin{aligned} E_p^{cart} &= 0 \\ E_p^{pend_1} &= m_{\mathrm{p1}} . g \cdot l_{\mathrm{p1}} \cdot \cos(\alpha) \\ E_p^{pend_2} &= m_{\mathrm{p2}} g (l_1 \cos(\alpha) + l_2 \cos(\theta)) \end{aligned}\right\} \tag{9}$$

Substituting energy equations in equation 1, the Lagrangian function of the system becomes:

$$\left.\begin{aligned} T = \frac{1}{2}\left(m_{\mathrm{c}} + m_{\mathrm{p1}} + m_{\mathrm{p2}}\right)\dot{x}_{\mathrm{c}}^2 + \frac{1}{2}\left(m_{\mathrm{p1}} l_{\mathrm{p1}}^2 + m_{\mathrm{p2}} l_1^2 + I_1\right)\dot{\theta}_1^2 + \frac{1}{2}\left(m_2 l_{\mathrm{p2}}^2 + I_2\right)\dot{\theta}^2 \\ + \left(m_1 l_{\mathrm{p1}} + m_2 l_1\right)\cos\alpha\, \dot{x}_{\mathrm{c}} \dot{\alpha} + m_2 l_{\mathrm{p2}} \cos\alpha\, \dot{x}_{\mathrm{c}} \dot{\theta} + m_2 l_1 l_{\mathrm{p2}} \cos(\alpha - \theta)\, \dot{\alpha}\dot{\theta} \\ - \left(m_1 l_{\mathrm{p1}} + m_2 l_1\right) g \cos\alpha - m_2 l_{\mathrm{p2}} g \cos\theta \end{aligned}\right\} \tag{10}$$

Using the obtained result for *T*, equations 3, 4 and 5 can be rewritten as follow:

$$\left.\begin{aligned} u = m_c \cdot \ddot{x}_c + \left(m_{p1} l_{p1} + m_{p2} l_1\right) cos\,\alpha\, \ddot{\alpha} + m_{p2} l_{p2} \cos\theta\, \ddot{\theta} - \\ \left(m_{p1} l_{p1} + m_{p2} l_1\right) sin\,\alpha\, \dot{\alpha}^2 - m_{p2} l_{p2} \sin\theta\, \dot{\theta}^2 \\ 0 = \left(m_{p1} l_{p1} + m_{p2} l_1\right) cos\,\alpha\, \ddot{x}_c + \left(m_{p1} l_{p1}^2 + m_{p2} l_1^2 + I_1\right)\ddot{\alpha} + \ddot{\theta} \\ m_{p2} l_1 l_{p2} \cos(\alpha - \theta) + m_{p2} l_1 l_{p2} \sin(\alpha - \theta)\, \dot{\theta}^2 - \left(m_{p1} l_{p1} + m_{p2} l_1\right) g \sin\alpha \\ 0 = m_{p2} l_{p2} \cos\theta\, \ddot{x}_c + m_{p2} l_1 l_{p2} \cos(\alpha - \theta)\, \ddot{\alpha} + \left(m_{p2} l_{p2}^2 + I_2\right)\ddot{\theta} - \\ m_{p2} l_{p2} g \sin\theta - m_{p2} l_1 l_{p2} \sin(\alpha - \theta)\, \dot{\alpha}^2 \end{aligned}\right\} \tag{11}$$

The equation 10 presents the compact matrix form of the last three equations:

$$\mathcal{H}(\gamma)\ddot{\gamma} + \mathcal{M}(\gamma,\dot{\gamma})\dot{\gamma} + \mathcal{F}(\gamma) = \mathcal{L}u \tag{12}$$

where:

$$\left.\begin{gathered} \gamma = (x_c \quad \alpha \quad \theta)^T \\ \mathcal{H}(\gamma) = \begin{pmatrix} a_1 & a_2\cos\alpha & a_3\cos\theta \\ a_2\cos\alpha & a_4 & a_5\cos(\alpha-\theta) \\ a_3\cos\theta & a_5\cos(\alpha-\theta) & a_6 \end{pmatrix} \\ \mathcal{M}(\gamma,\dot{\gamma}) = \begin{pmatrix} 0 & -a_2\sin\alpha\,\dot{\alpha} & -a_3\sin\theta\,\dot{\theta} \\ 0 & 0 & a_5\sin(\alpha-\theta)\,\dot{\theta} \\ 0 & -a_5\sin(\alpha-\theta)\,\dot{\alpha} & 0 \end{pmatrix} \\ \mathcal{F}(\gamma) = \begin{pmatrix} 0 \\ -\xi_1\sin\alpha \\ -\xi_2\sin\theta \end{pmatrix} \\ \mathcal{L} = (1 \quad 0 \quad 0)^T \end{gathered}\right\} \tag{13}$$

From Figure 1, it can be seen that the centre of mass of the rods is at the geometrical centre for both rods "l_{p1}" and "l_{p2}" will be "$l_1/2$" and "$l_2/2$" . As a result, parameters

$a_i(i = 1,2,\dots,6)$ will be defined as:

$$\left.\begin{gathered} a_1 = m_c + m_{p1} + m_{p2};\ a_2 = \left(\tfrac{1}{2}m_{p1} + m_{p2}\right) l_1 \\ a_3 = \tfrac{1}{2}m_2 l_2; a_4 = \left(\tfrac{1}{3}m_{p1} + m_{p2}\right) l_1^2 \\ a_5 = \tfrac{1}{2}m_{p2} l_1 l_2;\ \ a_6 = \tfrac{1}{3}m_{p2} l_2^2 \end{gathered}\right\} \tag{14}$$

$$\left.\begin{gathered} \xi_1 = \left(\tfrac{1}{2}m_{p1} + m_{p2}\right) l_1 g \\ \xi_2 = \tfrac{1}{2}m_{p2} l_2 g \end{gathered}\right\} \tag{15}$$

The nonlinear form of the state equation can be obtained by considering equation 12, multiplying it by the matrix $\mathcal{H}^{-1}(X)$, defining the state variables, and substituting those variables into the equation.

$$\left.\begin{gathered} \begin{bmatrix} \dot{X}_4 \\ \dot{X}_5 \\ \dot{X}_6 \end{bmatrix} = -\frac{\mathcal{M}(\gamma,\dot{\gamma})}{\mathcal{H}(\gamma)} \begin{bmatrix} X_4 \\ X_5 \\ X_6 \end{bmatrix} + \frac{1}{\mathcal{H}(\gamma)}\left[\mathcal{L}u - \mathcal{F}(\gamma)\right] \\ X_1 = x_c;\ X_2 = \alpha\ ;\ X_3 = \theta\ ;\ X_4 = \dot{x_c}\ ;\ X_5 = \dot{\alpha}\ ;\ X_6 = \dot{\theta}\ ; \\ \dot{X}_1 = X_4;\ \dot{X}_2 = X_5\ ;\ \dot{X}_3 = X_6;\ \dot{X}_4 = \ddot{x}_c;\ \dot{X}_5 = \ddot{\alpha}\ ;\ \dot{X}_6 = \ddot{\theta} \end{gathered}\right\} \tag{16}$$

The equation (16) could be written in a following compact form as well:

$$\dot{\mathrm{X}} = \begin{bmatrix} 0 & I \\ 0 & -\frac{\mathcal{M}(\gamma,\dot{\gamma})}{\mathcal{H}(\gamma)} \end{bmatrix} \cdot X + \begin{bmatrix} 0 \\ \frac{\mathcal{F}}{\mathcal{H}(\gamma)} \end{bmatrix} \cdot u + \begin{bmatrix} 0 \\ -\frac{\mathcal{F}(\gamma)}{\mathcal{H}(\gamma)} \end{bmatrix} \tag{17}$$

The Lagrangian function has been used to derive the dynamic model of the DIP system and the nonlinear form of the state equation. In the following section, the parameters in equation 16 will be identified through system identification of the DIP system. In order to identify the unknown parameters $(a_1, a_2, a_3, a_4, a_5, a_6, \xi_1, \xi_2)$, presented in equation 16, the online system identification will be conducted by applying the energy theorem. In order to solve for ai, equations must be formed. This requires collecting online data from the real system. In the following, the details of the DIP setup used in this project will be explained.

3 Swing-Up and Stabilisation of DIP

We used two control strategies to move the pendulum from its descending position to the vertical upright position and keep it there: one to swing up the pendulum and the other to balance the pendulum parts with a minimal amount of error for a rapid attainment of the dead position [8]. The state-space equation for the stance control system used was $\dot{z} = \mathcal{H} \cdot z + \mathcal{M} \cdot u + \mathcal{F}$, where the variables $\mathcal{H}$ and $\mathcal{M}$ are the system matrix and $\mathcal{H}$ is a concentrated disturbance that contains a disturbance due to an oscillating connection of the pendulum [9]. Thus, $z_e \in (e_z, \dot{e}_z)$ represented the error state vector, the desired state vector was z_d, and the actual state vector was $z_e = (z - z_d)$. The equation $\dot{z} = \Pi \cdot |z|^X \cdot sign(z)$ used differentiating sliding models $\dot{z} = \mathcal{k}^T \dot{z}_e$, and then, we substitute the actual state vector $\dot{z}_e = (\dot{z} - \dot{z}_d)$; therefore, we obtained the sliding model $\dot{z} = \mathcal{k}^T (\dot{z} - \dot{z}_d)$. If $z_d \in \left(\pm\frac{\pi}{2}\right)$ was the desired vector, the derivative vector was $\dot{z}_d \in (0,0)$. The conditions given above were to integrate the control $u = -\frac{1}{\mathcal{k}^T \mathcal{B}} \cdot [\mathcal{k}^T \mathcal{H} \cdot z + \Pi \cdot |z|^\beta \cdot sign(z)]$; it was swing-up control, and the exchanging gain Π was more noteworthy than the greatest furthest reaches of the $\mathcal{k}^T \mathcal{H}$ guarantee sliding [9]. The linear inverted pendulum system was a fourth-order system, and the state space was obtained with Equations (13) and (16), where $z \in \mathcal{R}^{4x1}, \mathcal{H} \in \mathcal{R}^{4x4}$, and $\mathcal{M} \in \mathcal{R}^{4x1}$. On the basis of the above equation, the incorporated control is $u = -\frac{1}{\mathcal{k}^T \mathcal{B}} \cdot [\mathcal{k}^T \mathcal{H} \cdot z + \Pi \cdot |z|^\beta \cdot sign(z) - \mathcal{k}^T \dot{z}_d]$ and the swing up control is presented [9].

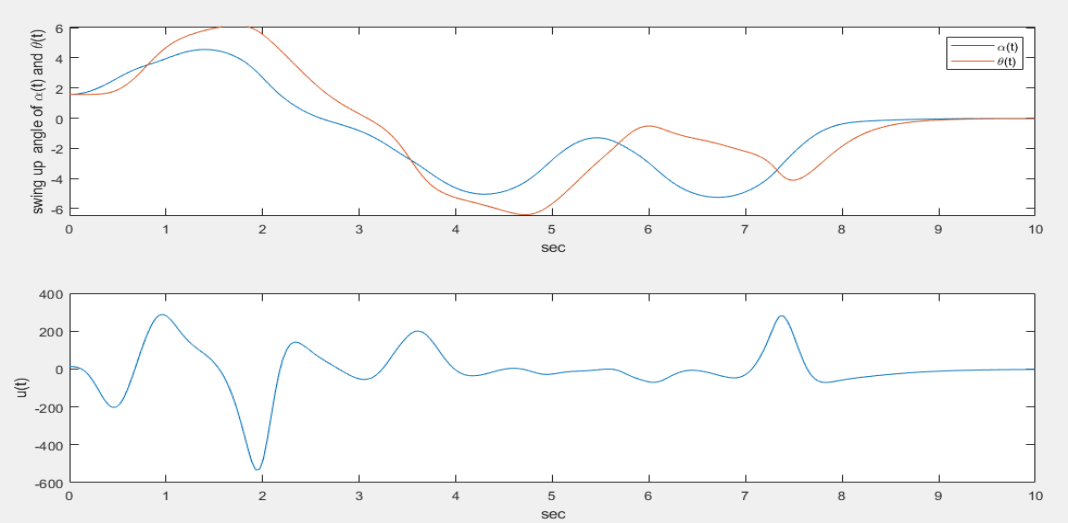


Fig. 2 Alpha and theta angle for the Swing up DIP

3 Simulation results in Matlab/Simscape

Simscape Multibody enables you to connect 3D mechanical models created in SolidWorks and simulate their dynamic behaviour. The process involves exporting a SolidWorks model as an XML file and then importing the XML file into Simscape Multibody. Once you have imported the XML file into Simscape Multibody, you can configure the model and create a simulation. You can then run the simulation to obtain results such as the motion of the parts [13], the forces between the parts, and the energy dissipated by the system. You can also add sensors and actuators, such as force and torque sensors, to measure the dynamic behaviour of the system. Simulation in Simscape Multibody from SolidWorks is an efficient and convenient way to analyse the dynamic behaviour of 3D mechanical structures. It enables you to assess the performance of your design, identify any potential problems, and make the necessary adjustments [10] quickly and accurately.

In the figure 3 and figure 3.a are presented the block diagram of the simscape model.

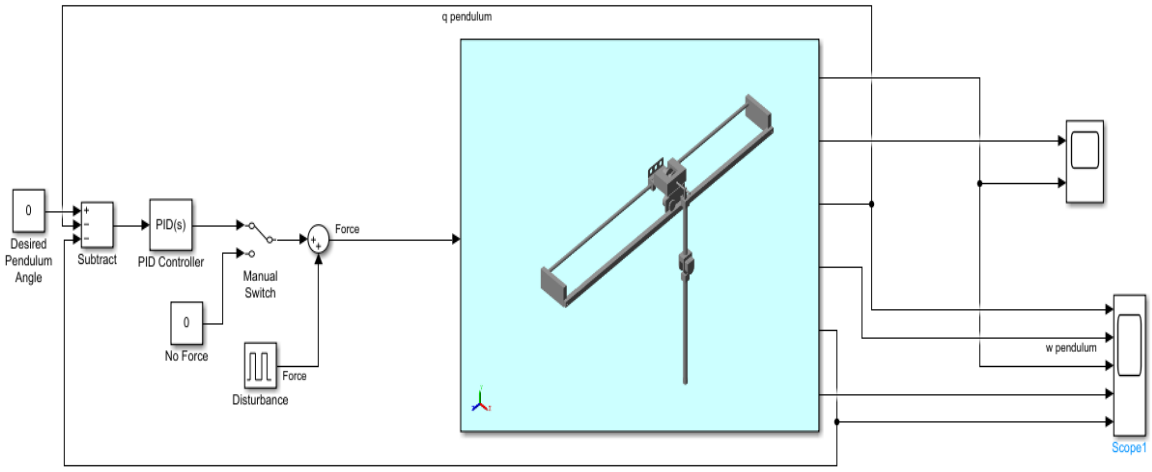


Fig. 3 Block diagram of MATLAB Simulink model for DIP system

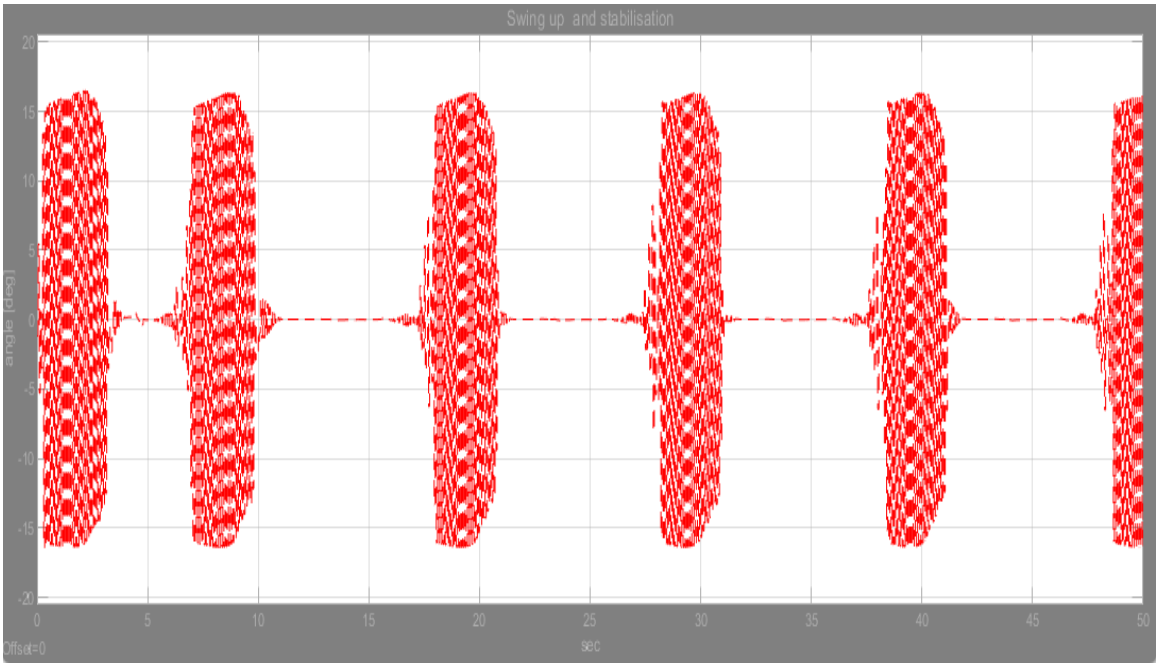


Fig. 3.a Stabilization of the DIP in Simscape

3 Experimental results on the QUARC Real-Time

This section explains the hardware and system components used to successfully build and balance the pendulum. Figure 4 shows the system setup used for this project.

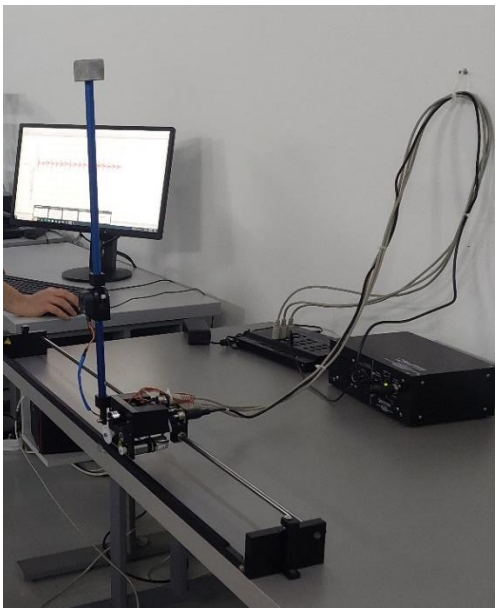


Fig. 4 Photo of the DIP at the Mechatronics lab/FME.

This section shows the experimental results of the combined sensitivity of our controller in comparison with PID-LQR and simulation. The platform of the DIP system is shown in Figure 12.

The experimental results are shown in Figures 5, 6, 7, 8, 9, 10, 11 and 12. Figure 5 shows LQR responses of the cart position x_c. Figure 6 and Figure 7 shows the responses of the pendulum angle $\boldsymbol{\alpha}$ and $\boldsymbol{\theta}$, Figure 8 and Figure 9 shows the responses of the pendulum angle velocity $\dot{\boldsymbol{\alpha}}$ and $\dot{\boldsymbol{\theta}}$. Figure 10 and Figure 11 shows the responses of the pendulum comparison angle $\boldsymbol{\alpha}$ and $\boldsymbol{\theta}$ between **LQR** and **PID** measured values. Figure 12 shows the responses comparison between simulated and measured values of amplifier voltage V_m.

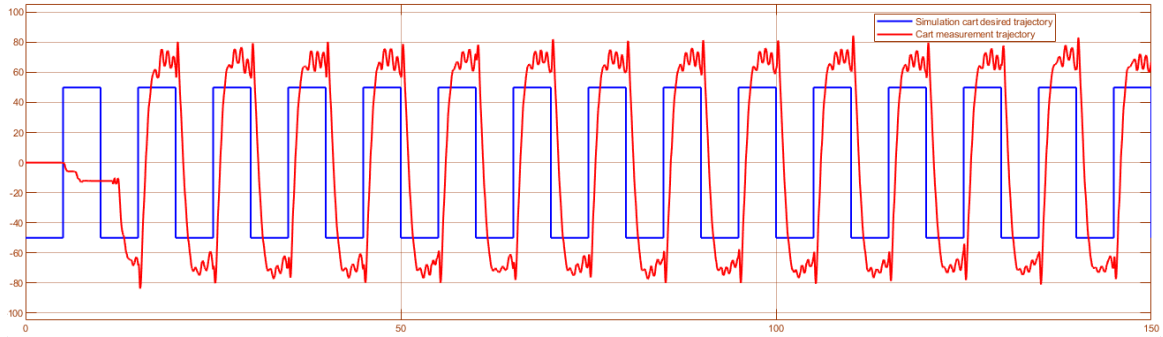


Fig. 5 Responses of the cart position x_c

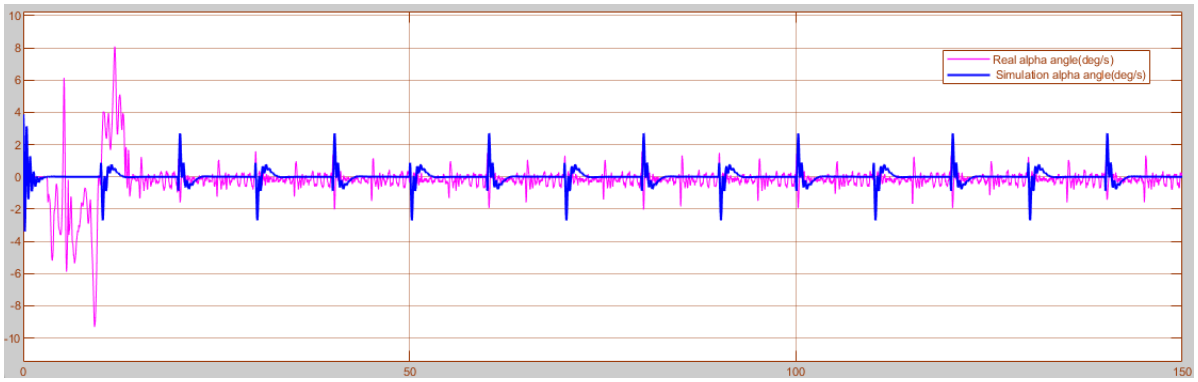


Fig. 6 LQR comparison between simulated and measured values of the pendulum angle $\boldsymbol{\alpha}$

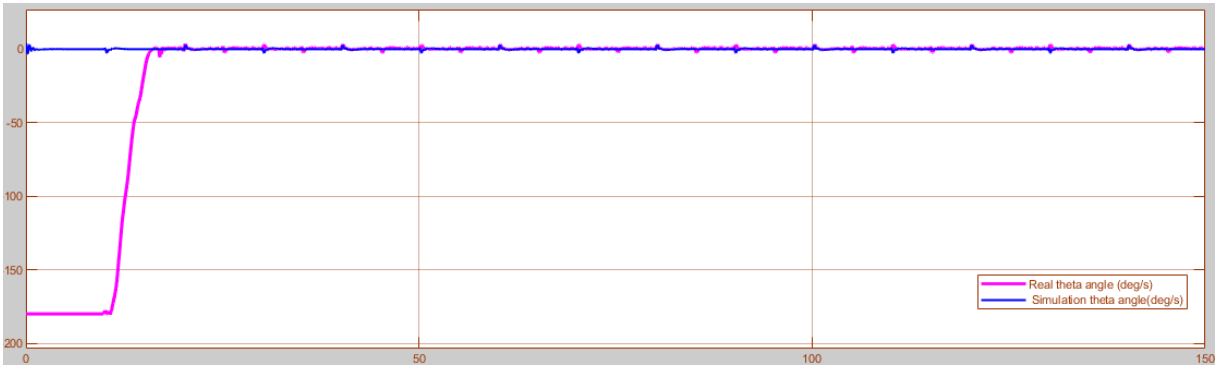


Fig. 7 LQR comparison between simulated and measured values of the pendulum angle $\boldsymbol{\theta}$

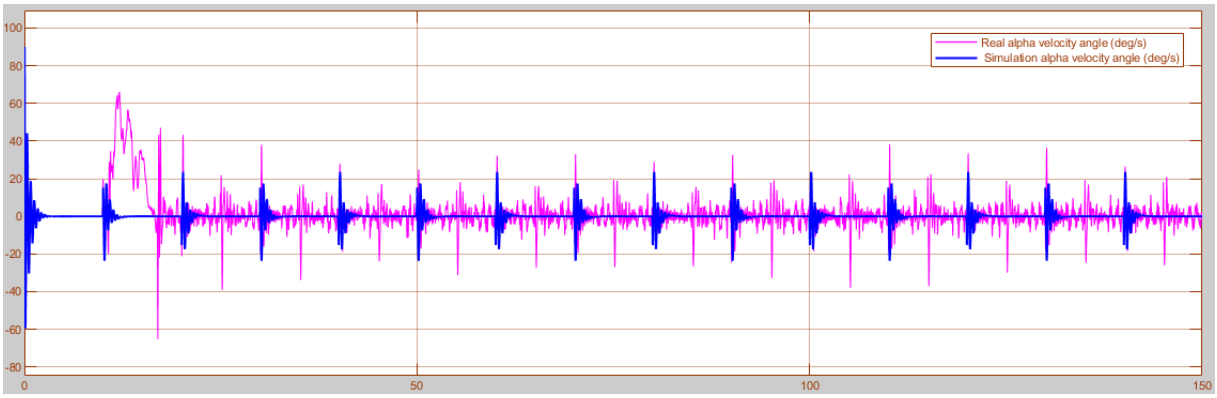


Fig. 8 LQR comparison between simulated and measured values of the pendulum angle $\dot{\boldsymbol{\alpha}}$

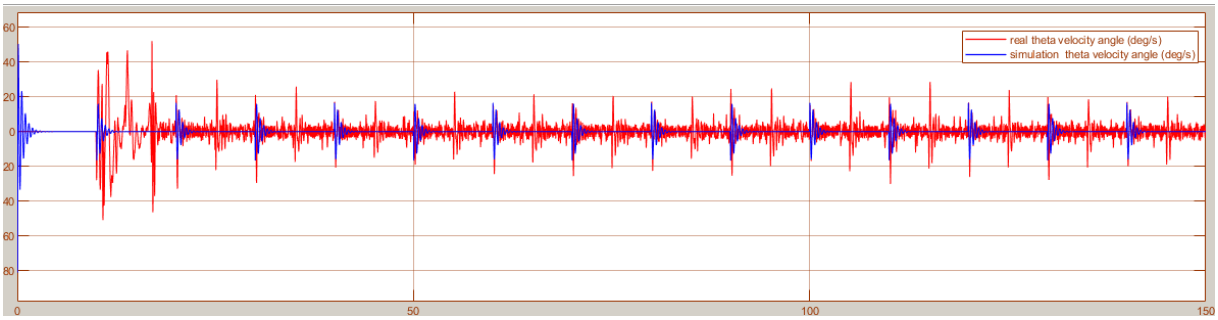


Fig. 9 LQR comparison between simulated and measured values of the pendulum angle $\dot{\boldsymbol{\theta}}$

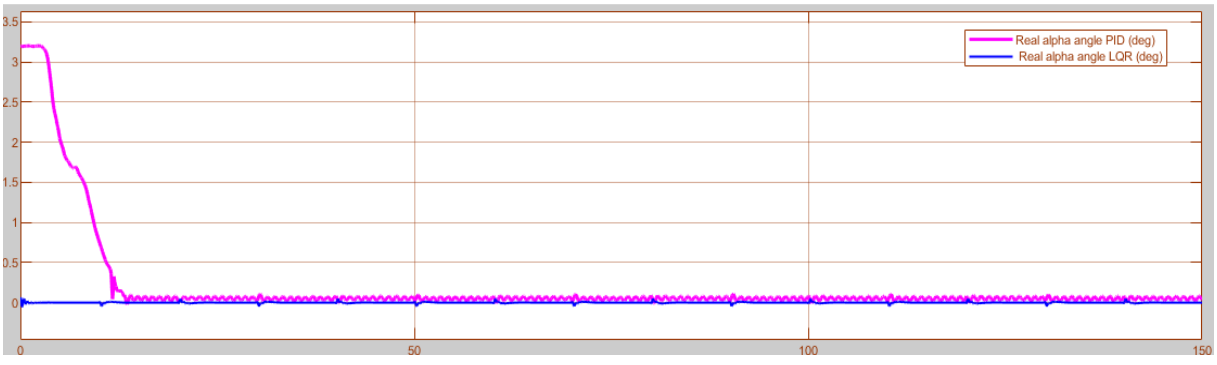


Fig.10 Comparison between LQR and PID measured values of the pendulum angle $\boldsymbol{\theta}$

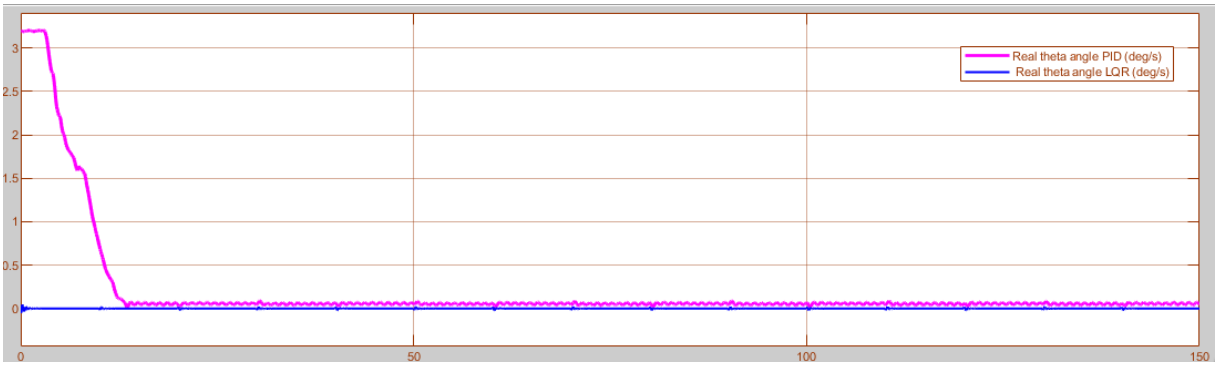


Fig. 11 Comparison between LQR and PID measured values of the pendulum angle $\boldsymbol{\alpha}$

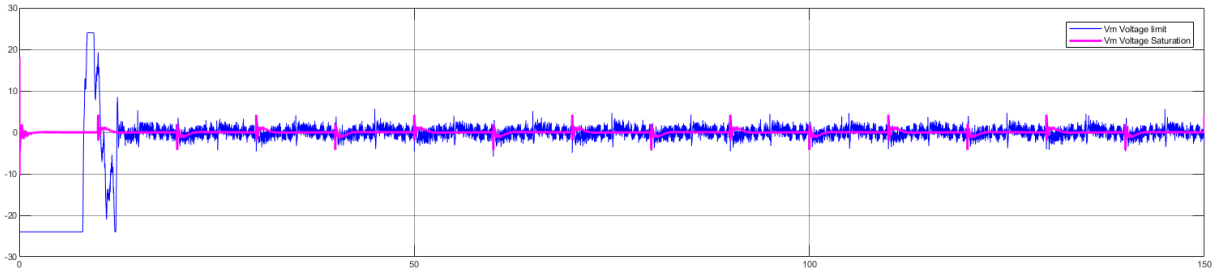


Fig. 12 Comparison between simulated and measured values of amplifier voltage V_m

CONCLUSION

This project presented an approach for designing a real-time control system for a double inverted pendulum using a combination of PID and LQR. The results of the real-time simulation showed that both the PID and LQR controllers were successful in swinging up and stabilizing the double inverted pendulum. This project also demonstrated the effectiveness of combining classical and modern control techniques to design a real-time control system for a complex, nonlinear dynamic system.

REFERENCES

[1] Li, Wende, Hui Ding, and Kai Cheng "An investigation on the design and performance assessment of double-PID and LQR controllers for the inverted pendulum", Proceedings of 2012 UKACC international conference on control. IEEE, **2012**.

[2] Abhijeet, L., Khubalkar S. W., Junghare, A. S. Modeling and control of fractional order PID controller fed rotary inverted pendulum.", 2018 International Conference on Power, Instrumentation, Control and Computing (PICC). IEEE, **2018.**

[3] Elkinany, B., Mohammed, A., Krafes, S., Chalh, Z. "Backstepping controller design with a quadratic error for a double inverted pendulum", International Journal of Modelling, Identification and Control 34 (1), pp. 33 – 40, **2020**.

[4] Kavirayani, S. "Novel Fuzzy Preview Control With Granular Computing for Underactuated Systems: Underactuated System Case Studies", In Handbook of Research on Emerging Applications of Fuzzy Algebraic Structures, pp. 352 – 368, IGI Global. **2020**.

[5] Hazem, Z. B., Bingül, Z. "A Study of Stabilization and Swing-up Linear Control for a Single Link Rotary Pendulum", In 2022 International Conference on Theoretical and Applied Computer Science and Engineering (ICTASCE), pp. 60 – 65, IEEE, **2022**,

[6] Yadav, S. K., Sharma, S., & Singh, N. “Optimal control of double inverted pendulum using LQR controller”, International Journal of Advanced Research in Computer Science and Software Engineering 2(2), **2012**.

[7] Quanser, Available online: https://www.quanser.com/products/rotary-inverted-pendulum (accessed on 10 May **2022**).

[8] Guo, X., Zhang, G., Tian, R., Periodic solution of a non-smooth double pendulum with unilateral rigid constrain. Symmetry 11(7), 886, **2019**.

[9] Bajrami, X., Pajaziti, A., Likaj, R., Shala, A., Berisha, R., Bruqi, M. “Control theory application for swing up and stabilisation of rotating inverted pendulum”, Symmetry 13(8), 1491, **2021**.

[10] Maki K., H., Ayankoso, S. A. “Modeling and Control of a Double Inverted Pendulum using LQR with Parameter Optimization through GA and PSO”, 21st International Conference on Research and Education in Mechatronics (REM), IEEE, **2020**.

[11] Bajrami, X., Shala A., Hoxha G., Likaj, R. “Dynamic Modelling and Analyzing of a Walking of Humanoid Robot”, Strojnícky časopis – Journal of Mechanical Engineering 68 (3), pp. 59 – 76, **2018**. DOI: 10.2478/scjme-2018-0027

[12] Likaj R., Shala, A. “Optimisation and Control of Vehicle Suspension Using Linear Quadratic Gaussian Control”, Strojnícky časopis – Journal of Mechanical Engineering 68 (1), pp. 61 – 68. **2018**. DOI: 10.2478/scjme-2018-0006

[13] Šlesar, P., Jančo, R. “The Calculation of the Contact Force and the Contact Width of Shaft Seals”, Strojnícky časopis – Journal of Mechanical Engineering 69(1), pp. 123 – 130, **2019**. DOI: 10.2478/scjme-2019-0010